Science of the Total Environment 756 (2021) 143593

Contents lists available at ScienceDirect

Science of the Total Environment

journal homepage: www.elsevier.com/locate/scitotenv

Effect of salinity on preconcentration of contaminants of emerging concern by nanofiltration: Application of solar photo-Fenton as a tertiary treatment

Dennis Deemter [a], Isabel Oller [a], Ana M. Amat [b], Sixto Malato [a,*]

[a] Plataforma Solar de Almería-CIEMAT, Carretera de Senés Km 4, Tabernas, Almería, Spain
[b] Grupo Procesos de Oxidación Avanzada, Campus de Alcoy, Universitat Politècnica de València, Spain

HIGHLIGHTS

- Microcontaminant permeability order was not influenced by increased salinity.
- Concentration factor is the key factor for permeability order and rate.
- Persulfate and hydrogen peroxide showed different elimination efficiencies.
- Persulfate was found inefficient for the elimination of selected microcontaminants.
- Solar photo-Fenton rapidly eliminated present and residual microcontaminants.

GRAPHICAL ABSTRACT

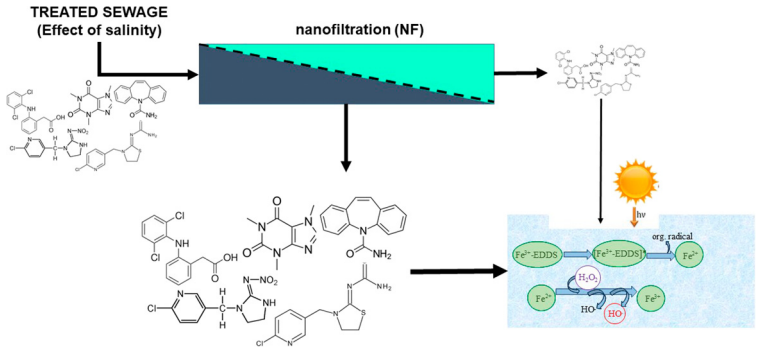

ARTICLE INFO

Article history:
Received 29 August 2020
Received in revised form 8 October 2020
Accepted 29 October 2020
Available online 17 November 2020

Editor: Dimitra A Lambropoulou

Keywords:
Microcontaminants
Nanofiltration
Salinity
Tertiary treatment
Solar photo-Fenton

ABSTRACT

This study focused on the effect of salinity on the performance of a pilot-scale nanofiltration (NF) for preconcentration of microcontaminants (MCs) in combination with solar photo-Fenton or photo-Fenton-like treatment for their elimination from NF permeate and concentrate streams. Photo-Fenton was carried out in a solar simulator at pH of 3 and at natural pH using Ethylenediamine-N, N′-disuccinic acid (EDDS) as an iron complexing agent. Degradation efficacy was tested with MCs commonly found in urban wastewater treatment plant effluents (caffeine, imidacloprid, thiacloprid, carbamazepine and diclofenac). Hydrogen peroxide and persulfate were compared in solar processes. Increase in salinity and pressure had a negligible influence on MC permeability order and NF selectivity. Solar photo-Fenton was able to degrade MCs present in the concentrated stream, and rapidly eliminate any residual MCs that might finally be present in permeate streams. Persulfate used instead of hydrogen peroxide was shown to be inefficient for the selected MCs. Fe(III):EDDS at circumneutral pH was able to remove MCs as quickly as classical photo-Fenton at acid pH, or even faster. This effect supports use of Fe(III):EDDS at natural pH for treating NF concentrates or polishing NF permeates when NF membranes are operated under extreme conditions of salinity.

1. Introduction

The worldwide need for clean water is increasing, while its availability rapidly decreases due to the effects of climate change, such as floods and draughts, rising population and widespread pollution by human

* Corresponding author.
E-mail address: sixto.malato@psa.es (S. Malato).

https://doi.org/10.1016/j.scitotenv.2020.143593

activity. Therefore, alternative sources of water must be found. Reused wastewater is highly promising as, depending on its final application, very high-quality water can be achieved [Ricart and Rico, 2019; Capocelli et al., 2019]. Growing populations, urbanization and industrialization are demanding higher production of detergents, food and pharmaceuticals [Li et al., 2016], increasing the overall salinity of NF influents [Abdel-Fatah, 2018]. Faster evaporation of water with rising temperatures will also lead to more rapid salination of soil and coastal groundwaters, and therefore, increasing salinity is also expected in UWWs.

Contaminants of Emerging Concern (CECs) are now being recorded for longer times, and microcontaminants (MCs) are increasingly found in urban wastewater (UWW) effluents in ranges from ng/L up to μg/L [Petrović et al., 2003]. Their origins can be found in the use and disposal of a variety of modern-day products, such as pesticides, pharmaceuticals and other organic compounds incorrectly disposed of, or which simply cannot be treated by conventional wastewater treatment plants [Rizzo et al., 2019]. Therefore, new treatment technologies are of the highest priority, while existing methods should be improved, scaled-up and combined to lower UWW treatment costs and prevent contaminants from passing through conventional wastewater treatment systems, resulting in bioaccumulation, chronic toxicity and endocrine disruption [McGinnis et al., 2019; Pico et al., 2019; Rasheed et al., 2019].

Several new perspectives on the problem of MCs passing through conventional wastewater treatments apply nanofiltration membranes (NF). This technology is relatively simple and inexpensive to apply, and consumes less power than current techniques, such as reverse osmosis [Mendret et al., 2019; Voigt et al., 2019]. Two groups of NF membranes, polymeric and ceramic, are widely used commercially. Polymeric NF membranes are used more often due to their lower cost, but have limitations regarding temperature, pH, fouling and cleaning. Although more expensive, ceramic membranes can be applied when the matrix pH is very high or low or temperatures are high, and they are easily cleaned by back-washing and/or incinerating the fouling layer. The main separating mechanism in the membrane technology is size exclusion, but also solution-diffusion and Donnan effect [Silva and Livingston, 2006; Zhang et al., 2019]. However, this can be strongly influenced by a variety of physicochemical mechanisms, such as molecular and surface polarity, pH, salinity and concentration polarization, as well as system parameters such as temperature, flow and pressure [Meschke et al., 2020]. Therefore, the effects of these mechanisms and parameters must be studied for a general understanding of the separation behavior of specific MCs during NF and its products, the concentrate and permeate streams.

In another perspective, Advanced Oxidation Processes (AOPs), which generate highly reactive, nonselective hydroxyl radicals ($^{\bullet}OH$), are applied to eliminate MCs [Kanakaraju et al., 2018]. One of these processes, photo-Fenton, is based on the catalytic iron cycle (Fe^{2+}/Fe^{3+}), promoted by hydrogen peroxide (H_2O_2) and UV–vis light to produce $^{\bullet}OH$. Its main advantage is that it uses simple chemicals and can be powered by solar radiation (renewable energy) with solar compound parabolic collectors already available [Janssens et al., 2019]. This has an important application potential in arid and semi-arid regions, due to their year-round high solar irradiation, where water reuse is also desirable due to its scarcity [UN DESA, 2019.].

One of the main drawbacks of photo-Fenton is that it must take place at pH 3 to maintain the iron in solution, which increases operating costs from pH adjustment when urban wastewater is to be treated. The use of a wide variety of iron complexing agents has been studied to avoid this. One of them, Ethylenediamine-N, N′-disuccinic acid (EDDS), makes solar photo-Fenton treatment possible at natural pH (pH = 7) by keeping iron soluble through formation of a stable photoactive complex. In addition, it should be mentioned that EDDS is not only photochemically effective, it is more photoreactive, because it is absorbent in a wider light wavelength which fits better to the solar UV–Vis spectrum, than conventional photo-Fenton [Dong et al., 2019]. Moreover, it is a biodegradable, environmentally-friendly substance [Tandy et al., 2006]. This information is confirmed by two recent review articles [Clarizia et al., 2017; and of Zhang and Zhou (2019). The primary transformation products of EDDS have been recently described [Jaber et al., 2020]. Six different products were identified and described as produced in the initial photo-redox process using lamps simulating solar spectrum. They are oxidized products with a shorter carbon chain than EDDS and aldehyde and/or carboxylic acid functions, proposing the formation of formaldehyde, which is likely to be further oxidized to formic acid. The authors state that these compounds are easily biodegradable and of low toxicity, not inducing them they would entail a greater risk of toxicity for the aquatic environment.

However, the high initial investment and high operating costs (mainly from reagents required) are still a drawback to its practical application. Therefore, solar photo-Fenton efficiency must be mapped over pretreated (UWW) effluents to guarantee its successful and efficient implementation as a tertiary treatment in existing systems, and increase the efficiency of recently developed hybrid systems using both NF and AOPs [Gallego-Schmid et al., 2019]. Focusing on this promising hybrid option, by increasing the MC concentration in the concentrate stream after NF pretreatment of UWW effluents, the total treatment volume could be reduced, significantly lowering reagents and accumulated UV energy required to attain the desired MC elimination percentage.

Thus, there is a pressing need for research on the effect of salinity on separation processes with NF membranes combined with AOPs in different UWW treatment plant (UWWTP) effluents. First the different physicochemical fouling mechanisms of NF membranes when filtering MCs from UWWTP effluents must be mapped. Salinity has already been shown to have an effect on concentration polarization, the formation of a gel-like layer or scaling induced by an accumulation of solutes, such as salts and MCs, near the membrane surface due to the surface polarity of commonly used NF membranes [Bi et al., 2016]. Preferential passage of the solvent through the membrane dramatically decreases the mass transfer coefficient of rejected ions, resulting in local supersaturation, while the bulk concentration in the matrix remains unsaturated [Shi et al., 2014; Song et al., 2018].

Pressure-driven filtration, and more specifically NF for MC removal, has been studied in detail in recent years addressing physicochemical properties of MCs (solute molecular weight/size/geometry, charge, and hydrophobicity), water quality conditions (pH, solute concentration, temperature, background inorganics, and natural organic matter), membrane properties and operating conditions (membrane fouling, membrane pore size, porosity, charge, and pressure) that influence the removal of MCs during membrane filtration [Kim et al., 2018; Patel et al., 2019]. The use of Solar photo-Fenton to treat MCs has been also deeply studied [Kanakaraju et al., 2018], however studies at circumneutral pH are still scarce [Ahile et al., 2020] and even more the use of persulfate as alternative to hydrogen peroxide at circumneutral pH [Wang and Wang, 2018a, 2018b; Ike et al., 2018]. Recently research in AOPs is dominated by the search for cost-effective and sustainable techniques [Miklos et al., 2018] but there is no study about how to combine NF with photo-Fenton at circumneutral pH for treating high salinity NF retentates containing MCs at realistic concentrations. Comparison of different operational variables of solar photo-Fenton process (by using Fe-EDDS) applied to eliminate MCs from both retentate and permeate has not been found in the revised literature. Therefore, this study focused on the effect of salinity on the performance of an NF system for preconcentration of MCs before solar photo-Fenton tertiary treatment for their elimination from natural water. Solar photo-Fenton was carried out at its optimal pH of 3 and at natural pH using EDDS as an iron complexing agent. The degradation efficacy of five MCs commonly found in UWWTP effluents, caffeine (CAF), imidacloprid (IMI), thiacloprid (THI), carbamazepine (CAR) and diclofenac (DIC) were tested in natural water spiked at a concentration of 100 μg/L each. Hydrogen peroxide and persulfate were compared as oxidizing

agents in solar photo-Fenton and photo-Fenton-like processes. Finally, the influence of different Fe:EDDS ratios was also evaluated.

2. Materials and methods

2.1. Reagents and chemicals

Target MCs (IMI, THI, CAR and DIC) were purchased from Sigma-Aldrich (Germany), except CAF, which was acquired from Fluka. NaCl was from Honeywell-Fluka. HPLC-grade solvents required for monitoring MCs were from Sigma-Aldrich. Iron substances, $FeSO_4 \cdot 7H_2O$ for Fe (II) and $Fe_2(SO_4)_3 \cdot xH_2O$ for Fe(III), as well as Sodium persulfate ($Na_2S_2O_8$) and H_2O_2 (35% *w*/*v*) were also from Sigma Aldrich. H_2SO_4 (95–97%) was from J.T. Baker. The water matrix was natural water (Tabernas, Spain) (see Table SI 1 for composition). Fig. 1 is a schematic overview of the five MCs selected.

2.2. Analytical determinations

MC concentrations were measured by ultra-performance liquid chromatography (UPLC) using an Agilent Technologies 1200 series device, with a UV-DAD detector and a Poroshell 120 EC-C18 column (3.0 × 50 mm). The starting eluent conditions, 95% water with 25 mM Formic acid (mobile phase A) and 5% ACN (mobile phase B) at 1 mL/min, were kept for 5 min. Then, a linear gradient progressed for 10 min to 68% ACN and kept at this concentration for 2 min. The injection volume was 100 μL at a temperature of 30 °C. Samples were prepared by adding 1 mL of ACN to 9 mL of this mixture and then filtered through a hydrophobic PTFE 0.2 μm (Millipore Millex-FG) syringe filter into a 2-mL HPLC vial. Table SI 2 shows the molecular weight, retention time, limit of quantification (LOQ) and maximum absorption wavelength of each target MC. Dissolved organic and inorganic carbon (DOC and IC) were measured with a Shimadzu TOC-VCN analyzer. H_2O_2 was determined directly after sampling using Titanium (IV) oxysulfate following DIN 38402H15. Iron was determined after filtering through a 0.45 μm Nylon filter, using 1,10 phenanthroline following ISO 6332. Persulfate determination was adapted from Liang [Liang et al., 2008].

2.3. Experimental set-up

2.3.1. NF membrane pilot plant

The NF pilot plant (Fig. 2) consisted of a 400-L feed tank equipped with a recirculation pump to ensure that the concentrate stream was continuously mixed with the tank volume, and the MC concentration increased as the volume was reduced by permeate discharge. The feed tank pump was a single multistage centrifugal pump with a frequency modulator for pressure generation and internal recycling. NF membranes were DOW FILMTEC™ NF90–2540, rolled-sheet polyamide thin-film composite membranes, which work by crossflow filtration. NF membranes have a total surface area of 5.2 m^2 and are operable at up to 45 °C, in pH 2–11, a maximum operating pressure of 41 bars and molecular weight cut-off (MWCO) of 250.0 g/mol. Like most commercial NF membranes, the surface is negatively charged [Zhang et al., 2020]. The system includes three digital flow meters (measuring permeate, concentrate and recycle flows), two conductivity meters (measuring the conductivity of permeate and concentrate streams in μS/cm and mS/cm, respectively), two pressure sensors (before and after the membrane unit; measuring in bars) and a temperature sensor in the recirculation circuit (°C). All values are integrated in a SCADA user interface. The maximum system pressure was set at 10 bars.

2.3.2. Experimental procedure

A stock solution of the MC mixture containing CAF, IMI, THI, CAR and DIC was prepared in methanol to a concentration of 2.5 g/L of each compound, ensuring high solubility and low TOC later, when diluted in water to a μg/L range. The desired matrix was prepared in the feed tank to a final concentration of 3, 5 or 7 g/L of NaCl and 100 μg/L of each MC in order to work close to the actual content usually found in MWWTP effluents. The system was operated at 5, 7 and 10 bars. The first permeate sample (P1) was collected after operating the NF plant for 180 min, the point of concentration polarization, as mentioned in the Introduction. The resulting volume was approximately 100 L of permeate. The second permeate sample (P2) was taken after an additional 660 min of batch operation. The concentrate stream (C1) was collected after attaining a CF of 2.7. All samples (5 L) were stored in separate bottles and kept refrigerated until further use. MC concentrations and main physicochemical parameters of each sample may be found in Table 1.

2.3.3. Solar photo-Fenton treatment

Solar photo-Fenton experiments were performed with a solar simulator (Atlas-SunTest XLS+) with a daylight filter, and a xenon lamp on the chamber ceiling, programed for total radiation of 365 W/m^2 (300–800 nm) and 30 W/m^2 of UV radiation (300–400 nm) under continuous ventilation to keep the temperature at 25 °C. A magnetically stirred cylindrical 1-L container (18.5 cm diameter and 4.0 cm deep) was placed in the center inside the solar simulator chamber.

Classic photo-Fenton experiments at pH 3 were carried out with 1 L of sample (P1, P2, C1) acidified with H_2SO_4 to pH 3 prior to the addition of $FeSO_4 \cdot 7H_2O$. For the experiments at natural pH, carbonates/bicarbonates (known $^{\bullet}OH$ radical scavengers) were removed by air stripping after addition of H_2SO_4, lowering the total inorganic carbon to 15 mg/L. The Fe^{3+}-EDDS ratio ($Fe_2(SO_4)_3.7H_2O$ previously dissolved in demineralized water at pH 3, followed by addition of EDDS) was 1:2 for all experiments. The starting iron concentration was 0.10 mM and the H_2O_2 concentration was 1.50 mM. In the experiments at natural pH, the EDDS concentration was 0.20 mM. Starting photo-Fenton conditions were selected based on previous results [Klamerth et al., 2010; Miralles-Cuevas et al., 2013]. Further experiments with variations on the parameters given here were also performed: iron concentration doubled to 0.20 mM, EDDS concentration in 0.10 mM halved and persulfate instead of H_2O_2 at equal concentrations. For an overview of those experiments see Table SI 3.

3. Results and discussion

3.1. Effect of salinity on nanofiltration membranes

The differences in influence of the two water matrices (demineralized water and natural water (Tabernas, Spain)), system

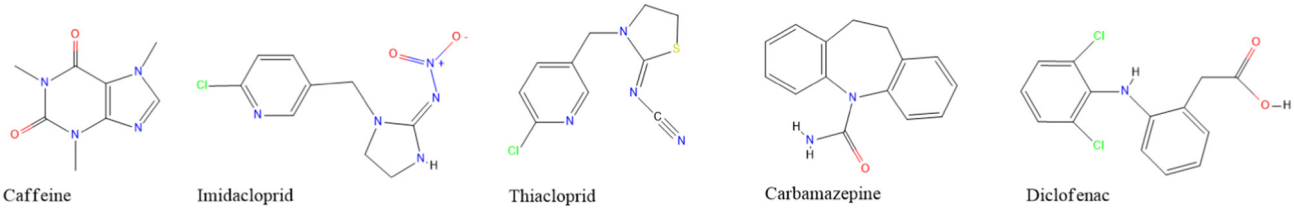

Fig. 1. Schematic overview of the molecular structures of CAF, IMI, THI, CAR and DIC. The molecular charge is shown in red (negative), yellow (moderate negative), blue (positive) or green (neutral).

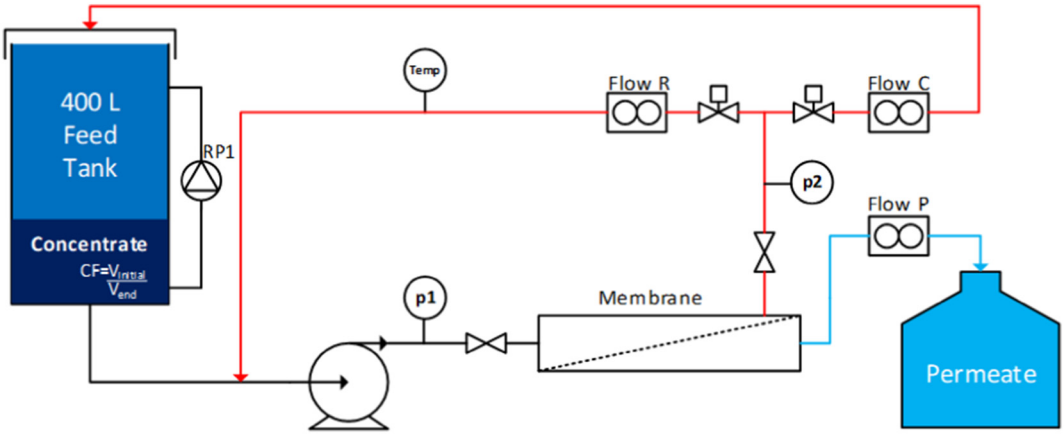

Fig. 2. Schematic overview of the NF pilot plant. 'Temp' is the temperature sensor in the recirculation circuit, 'Flow R, C and P' are the recycle, concentrate and permeate stream digital flow meters, respectively; p1 and p2 are the pressure meters before and after the membrane. The feed tank is equipped with a recirculation pump (RP1). The concentration factor (CF) can be determined by dividing the starting volume (V_{start}) by the end volume (V_{end}).

pressure (5, 7 and 10 bars), and salinity (3, 5 and 7 g/L of NaCl) were assessed in the NF pilot plant. Water matrices were spiked with target MCs from the stock solution to reach the starting feed tank concentrations of 100 μg/L, each. Total experimental time was set at 360 min when demineralized water was tested, which was the time required to attain the desired maximum concentration factor of 4 (CF = 4.0). It should be mentioned that high concentrations of the permeating THI, CAF and CAR were already detected at this stage. During all experiments with the demineralized water matrix, with and without addition of NaCl and at different pressures, permeability of three MCs, THI, CAF and CAR was detected when in operation for over 180 min. This point was therefore set as the membrane surface saturation point time, which is also called the concentration polarization point as described in the Introduction.

In all the experiments, the order of MC membrane permeability was THI, CAF, and CAR with very low concentrations of DIC. This can be explained due to their molecular morphology (see Fig. 1 in Section 2.1), flexibility and weight (252.7, 194.2 and 236.3 g/mol, respectively; DIC 318.1 g/mol; membrane MWCO 250.0 g/mol). Positively charged molecules also significantly promote MC membrane permeability, as the membrane surface is negatively charged (see details in 2.3.1), attracting the positively charged molecules, instead of repelling them. MC increases in the concentrate stream were inversely related to the concentration factor (CF). In addition, as expected, higher NF pilot plant system pressure resulted in higher CFs.

In experiments with addition of 3 g/L of NaCl, the same pressures as in the previous experiments were evaluated. MC permeability through NF membrane showed the same order as without the addition of NaCl. DIC was again not detected in the permeate stream and the rest of MC membrane permeability order remained the same as observed with demineralized water alone (THI, CAF and CAR).

Table 2, shows the time needed to reach 10 μg/L per MC in the permeate stream. Under these conditions, it was possible to obtain a CF of 2.0, 3.0 and 4.0 at 120, 180 and 300 min, respectively, only at 10 bars. At lower pressures, for instance, at 5 bars, a CF of 2.0 was only reached after 420 min. Similarly, salinity (measured as conductivity) increased by a factor of 2.0 in the feed tank at 180, 150 and 90 min, at 5, 7 and 10 bars, respectively.

The system pressure applied was set at 10 bars, because that is the maximum NF pilot plant system pressure, however, higher pressures are more likely to be used in future commercial applications. Especially, at higher salinity, such as with the addition of 5 and 7 g/L of NaCl to the matrix, this low pressure prevented the desired CF of 4 from being reached within the experimental time, which was set at 360 min (data not shown). For instance, with demineralized water and 5 g/L of NaCl at 10 bars, it was only possible to reach a CF of 2.0 and 3.0 at 210 and 360 min, respectively.

Continuing with our objective of assessing the effect of salinity on nanofiltration membranes, the next step was to increase the complexity of the water matrix by using natural water (Tabernas, Spain, physicochemical characterization in Table SI 1). From this point on, IMI was included in the mixture of MCs, as described in Section 2.3.2, because five MCs could provide more variability in NF permeability and retention, enriching the results. Like THI, IMI is one of the neonicotinoids, a group of widely used pesticides that has been showing high persistency in the environment and is increasingly held responsible for the elimination of bees around the world [Kessler et al., 2015; Brandt et al., 2016].

Although the use of natural water as a matrix made the salinity higher than demineralized water, because it also contained salts other than NaCl, no differentiation in MC membrane permeability order, as previously described, was observed after the addition of 3, 5 and 7 g/L NaCl. Total matrix salinity after addition of NaCl was 8200, 11,100 and 14,500 μS/cm, respectively.

Fig. 3 shows the evolution of the total MC concentration in the permeate and concentrate (inset) streams during the full experimental time of 360 min. Final MC increment in the permeate stream was 25.7, 3.2 and 3.8 times higher compared to demineralized water experiments and in the concentrate stream 2.3, 1.7 and 1.4 times higher, with 3, 5 and 7 g/L NaCl added, respectively.

Table 1
MC concentration [mg/L] and main physicochemical parameters of each stored sample: Permeate samples (P1 and P2) were collected after NF plant and concentrate stream (C1) was collected after attaining a concentration factor (CF) of 2.7.

	CAF	IMI	THI	CAR	DIC	pH	IC [mg/L]	Conductivity [mS/cm]
P1	0.0091	0.0198	0.0238	0.0050	0.0050	*8.3*	*14.0*	*2.4*
P2	0.0321	0.0505	0.0561	0.0101	0.0079	*8.8*	*25.4*	*6.5*
C1	0.2344	0.1927	0.1692	0.2568	0.2199	*8.9*	*253.8*	*27.8*

Table 2
Time needed to reach 10 μg/L of each MC in the permeate stream in demineralized water with 3 g/L NaCl.

Pressure, bars	5	7	10	
THI	180	150	120	min.
CAF	420	300	210	min.
CAR	–	–	300	min.
DIC	–	–	–	min.

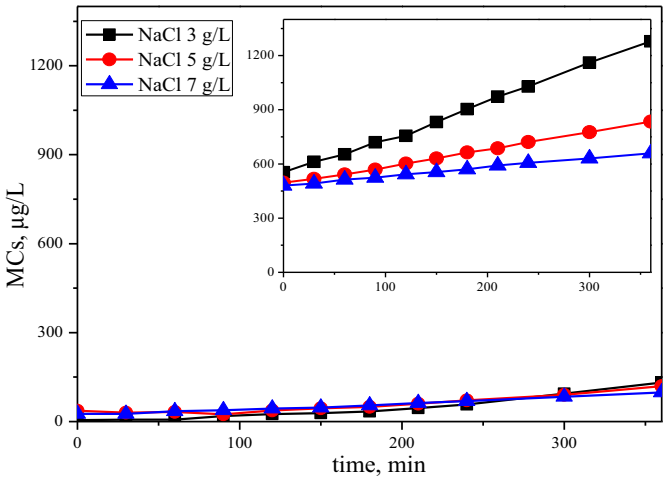

Fig. 3. Concentration over time of the sum of MCs in the permeate and concentrate (inset) streams, after addition of 3, 5 and 7 g/L NaCl to natural water.

When 3 g/L NaCl were added, the permeate and concentrate conductivities at $t = 0$ min were 430 and 10,500 µS/cm, respectively, increasing to 2400 and 20,200 µS/cm at $t = 360$ min (end of experiment). Thus, after 360 min, salinity had increased by a factor of 5.7 in the permeate stream, 2.3 in the tank and 1.9 in the concentrate stream, and the CF was 3.3. After adding 5 g/L NaCl, permeate and concentrate stream conductivities at t = 0 min were 650 and 13,700 µS/cm, respectively, increasing to 4300 and 21,400 µS/cm at t = 360 min. Also after 360 min, salinity in the permeate stream had increased by a factor of 6.5, 1.8 in the tank and 1.6 in the concentrate stream, and the CF was 2.4. Finally, 7 g/L NaCl added to the permeate and concentrate led to conductivities at t = 0 min of 1400 and 17,900 µS/cm, respectively, increasing to 4600 and 22,700 µS/cm at t = 360 min. Salinity in the permeate stream increased by a factor of 3.2, 1.5 in the tank and 1.3 in the concentrate. After 360 min, the CF was 1.6, a clearly significant decrease in the concentration capacity of the NF system employed in this study, as a CF near 4 was only attained with addition of 3 g/L NaCl to the natural water which already had a starting conductivity of 2300 µS/cm.

In all the experiments, the MC membrane permeability order was IMI, THI, CAF and CAR. DIC was not detected in the permeate stream. This is mainly due to the molecular weight of the MCs and their molecular charge as explained above. Growing CF, and thus salinity, was observed with more MCs, and THI and IMI especially increased disproportionately in the permeate stream. It may therefore be concluded that higher salinity resulted in decreased membrane efficiency and MC retention. Based on this conclusion, and for the main objective of simulating the most unfavorable operating conditions, the rest of experiments were carried out with the addition of 7 g/L NaCl at a system pressure of 10 bars. Under these conditions, after 360 min, the total MC concentrations were 104 µg/L (IMI: 30 µg/L, THI: 39 µg/L, CAF: 19 µg/L, CAR: 11 µg/L and DIC: 5 µg/L) and 659 µg/L (IMI: 130 µg/L, THI: 129 µg/L, CAF: 156 µg/L, CAR: 162 µg/L and DIC: 82 µg/L) in permeate and concentrate streams, respectively. The final concentration in the feed tank was 659 µg/L.

After evaluating the effect of salinity on NF system performance, several batches were run to produce enough concentrate and permeate for further tertiary treatment by solar photo-Fenton. Batches were generated at an isobaric system pressure of 10 bars. Natural water (Tabernas, Spain) with a starting concentration of 7 g/L NaCl was used, as it was the highest salinity tested in the previous experiments and high saline effluents from actual UWW are the main target of this combined technology. Furthermore, as NF was proposed to concentrate MCs, it was tested under conditions that were not so mild in order to obtain more conservative (not optimistic) results. For Batch P1, the NF plant was operated with a starting volume of $V_0 = 400$ L for 180 min, as permeability of the four MCs IMI, THI, CAF and CAR was detected at over 180 min. The resulting volume after 180 min of Batch P1 was $V_{P1} = 100$ L of permeate. NF plant operation continued with the remaining 300 L for another 660 min, resulting in Batches P2 and C1 having equal volumes of $V_{P2} = V_{C1} = 150$ L. This longer operation time than the previous 360 min was selected because a final batch volume ratio close to 4 was desired. These batches (P1 and P2 for permeates with different low concentrations of MCs and C1 for high concentration of MCs) were prepared for later treatment with solar photo-Fenton under different operating conditions. The main objective defined for all the different treatments applied to permeate and concentrate streams was 90% degradation of the sum of MCs. This is an ambitious objective in view of the new regulation in Switzerland (the only country in Europe, for the moment, specifically regulating MCs in UWWTP effluents), which requires 80% of CECs to be eliminated from raw wastewater (Eggen et al., 2014).

3.2. Solar photo-Fenton tertiary treatment

3.2.1. Conventional solar photo-Fenton treatment at pH 3

The starting conditions for photo-Fenton treatment were selected based on previous results and low initial concentrations of Fe(II) and H_2O_2 to reduce the environmental and economic impacts, while still providing high elimination efficiency with a wide range of MCs [Klamerth et al., 2010; Miralles-Cuevas et al., 2013].

Fig. 4 shows the results for samples P1, P2 and C1 with mild experimental parameters for solar photo-Fenton at pH 3 (0.10 mM Fe(II) and 1.50 mM H_2O_2).

Fig. 4 shows that in sample C1, elimination of CAF, CAR and DIC to below the LOQ (5 µg/L) took less than 5 min of treatment. Although IMI and THI showed higher persistence to solar photo-Fenton, more than 70% was eliminated after 30 min. H_2O_2 consumption at the end of the experiment was 0.70 mM (around 50% of the starting amount). First order kinetic constant (r = kC) were 0.770 min^{-1}, 0.042 min^{-1}, 0.041 min^{-1}, 0.793 min^{-1}, 0.737 min^{-1} for CAF, IMI, THI, CAR and DIC, respectively.

In samples P1 and P2, CAF, CAR and DIC were eliminated to LOQ (5 µg/L) quite fast within the first 5 min of treatment. Indeed, DIC was degraded by Fenton in the dark ($t < 0$), even before illumination. IMI and THI showed higher persistence in solar photo-Fenton than the other MCs, and only 90% was eliminated from P1 and P2 after 25 and 30 min, respectively. First order kinetic constant for P1 were 0.133 min^{-1}, 0.060 min^{-1} and 0.071 min^{-1}, for CAF, IMI and THI,

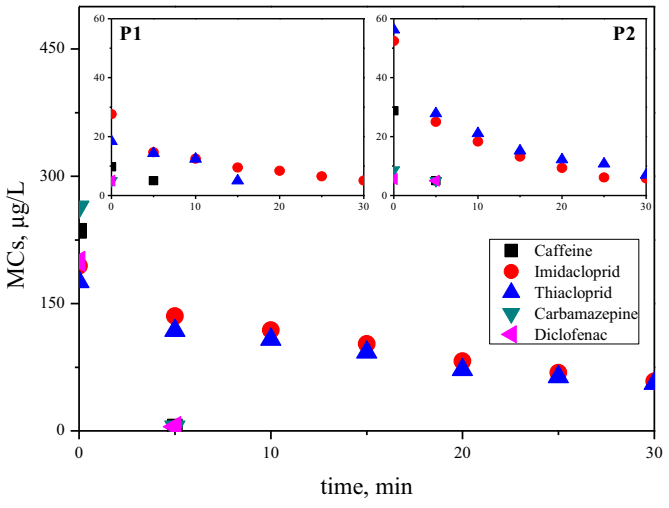

Fig. 4. MC concentrations during solar photo-Fenton treatment at pH 3 of concentrate C1. Insets show results of P1 and P2 tertiary treatments.

respectively. And 0.350 min^{-1}, 0.083 min^{-1} and 0.074 min^{-1}, for CAF, IMI and THI, respectively, for P2.

H_2O_2 consumption at the end of the experiments was 0.50 mM and 0.80 mM, respectively. Therefore, H_2O_2 consumption was not affected by MC concentration, and was very similar in P1, P2 and C1. Treatment of concentrates was slower but successful as degradation was over 90% of the sum of MCs after 20 min of treatment, and always over 70% for individual MCs after 30 min.

3.2.2. Solar photo-Fenton at natural pH using EDDS

Mild solar photo-Fenton at natural pH (0.10 mM Fe(III):EDDS; [1:2] and 1.50 mM H_2O_2) was also applied to samples P1, P2 and C1 (results shown in Fig. 5). Starting photo-Fenton parameter values were selected based on previous studies with low starting concentrations of Fe(II) and H_2O_2 [Miralles-Cuevas et al., 2014].

Elimination *of CAF, CAR and DIC to* LOQ (5 μg/L) *was attained* in C1 in less than 5 min. More recalcitrant MCs (IMI and THI) were degraded 90% in less than 15 min. The decay of Fe(III):EDDS has been described as parallel to evolution of dissolved Fe, as stated by other studies using Fe(III):EDDS where the complex was evaluated in detail [Soriano-Molina et al., 2018; Costa et al., 2020]. Iron precipitation (when the complex was degraded) started to be detected at just under 20 min, with a total loss of 0.03 mM of dissolved iron after 30 min. H_2O_2 consumption was around 1.20 mM after 30 min, but 0.80 mM at 15 min, when 90% degradation was attained. First order kinetic constant were 0.768 min^{-1}, 0.150 min^{-1}, 0.126 min^{-1}, 0.792 min^{-1}, 0.732 min^{-1} for CAF, IMI, THI, CAR and DIC, respectively.

As seen in Fig. 5, in samples P1 and P2, elimination of all MCs to LOQ (5 μg/L) was rapidly achieved. Within less than 5 min, all MCs were degraded 90%. Iron precipitation due to EDDS degradation began after 10 min and was fully precipitated at 30 min of treatment. *Consumption of* H_2O_2 was 1.20–1.30 mM at the end of the experiment, but as low as 0.60 mM after 5 min. Therefore, H_2O_2 consumption was not affected by MC concentration, but naturally decomposed during the treatment time. First order kinetic constant for P1 were 0.137 min^{-1}, 0.266 min^{-1} and 0.304 min^{-1}, for CAF, IMI and THI, respectively. And 0.386 min^{-1}, 0.269 min^{-1} and 0.192 min^{-1}, for CAF, IMI and THI, respectively, for P2. Fe(III):EDDS at circumneutral pH was able to rapidly eliminate MCs in the NF samples, at least as efficiently as classic photo-Fenton at acid pH, or even more so, as stated by first order kinetic constants of the different MCs. IMI and THI were the most recalcitrant MCs in both treatments.

Test were done in water containing high chloride concentration, without any special detrimental effect on the photo degradation of MCs. Lado Ribeiro et al. (2019) reviewed the effects for different AOPs due to the main components present in wastewater, describing the formation of less reactive radicals than hydroxyl ($Cl_2^{\bullet-}$). Regarding chloride anions at high concentration it was reported (Soriano-Molina et al., 2019) not any effect or slight improvement in the reaction rate due to the intervention of chlorine radicals on MCs degradation.

3.2.3. Effect of operating parameters on solar photo-Fenton tertiary treatment at pH 3

Sulfate has previously been reported to decrease photo-Fenton efficiency, as it scavenges hydroxyl and other radicals [De Laat et al., 2004; Zapata et al., 2009; Lado Ribeiro et al., 2019]. When the matrix was acidified to pH 3, the sulfate concentration was almost four times higher than at pH 7. Therefore, the higher reaction rate attained with Fe(III):EDDS at natural pH than with photo-Fenton at pH 3 could be related to hydroxyl radical scavenging by sulfate.

In an attempt to neutralize the negative effect of radical scavenging by sulfate, another 0.60 mM of H_2O_2 was added after 15 min (pH 3). *Elimination of CAF, CAR and DIC* to LOQ (5 μg/L) *was obtained in less than 5 min, while* IMI and THI had still not reached *90%* elimination after 30 min. *No positive effect of the second addition of* H_2O_2 *on elimination of contaminants was observed, especially in view of the same consumption of* H_2O_2 (0.70 mM) as in the experimental results shown in Fig. 4.

In a similar attempt to improve solar photo-Fenton at pH 3, a double concentration of iron (0.2 mM) was also tested. Fig. 6 shows *elimination* to LOQ (5 μg/L) *of CAF, CAR and DIC in the first 5 min.* After 30 min of treatment, 85% and 80% of IMI and THI, respectively, was eliminated. First order kinetic constant were 0.766 min^{-1}, 0.067 min^{-1}, 0.061 min^{-1}, 0.800 min^{-1}, 0.712 min^{-1} for CAF, IMI, THI, CAR and DIC, respectively. The positive effects of the increased iron concentration were minimal (compare first order kinetic constants calculated from results in Fig. 4), and H_2O_2 consumption was 0.95 mM at 30 min, 20% higher than the basic experimental parameters (Fe 0.10 mM and 1.50 mM H_2O_2). In addition, after 5 min of treatment, H_2O_2 consumption was 0.36 mM, more than double with 0.10 mM Fe(II). Therefore, the

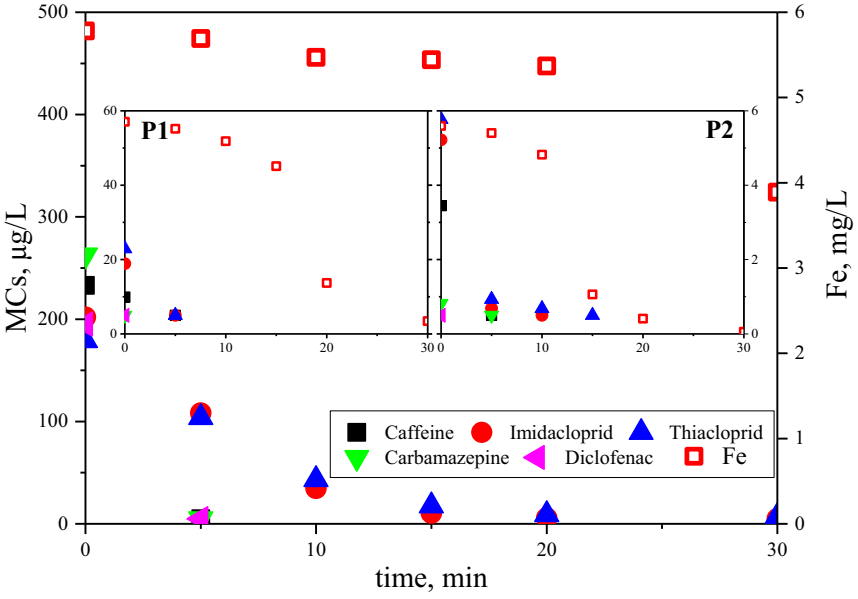

Fig. 5. MC concentrations and dissolved iron evolution during solar photo-Fenton with Fe(III):EDDS [1:2] at natural pH (pH = 7) in concentrate C1. Insets show results with P1 and P2.

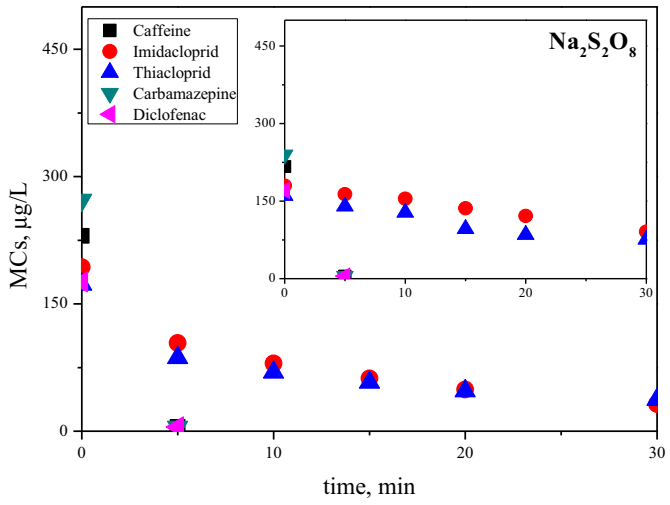

Fig. 6. MC concentrations during solar photo-Fenton at pH 3 (0.20 mM Fe(II) and 1.50 mM H_2O_2) in Concentrate C1. The inset shows the results with persulfate (1.5 mM) as the oxidizing agent.

higher reaction rate with Fe(III):EDDS at natural pH than at pH 3 could not be justified by a lack of oxidizing radicals provoked by a low iron concentration, but could be due to the high concentration of sulfate in C1 which scavenged hydroxyl and other radicals or may be related with the different photoreactivity of iron species formed with Fe(III):EDDS at natural pH or at pH 3.

Finally, persulfate was used as an alternative to H_2O_2 just to check the possibility of improving traditional solar photo-Fenton treatment of C1 at pH 3. The use of persulfate in photo-Fenton has been described previously elsewhere. [Wang and Wang, 2018a, 2018b; Wang et al., 2019] The added persulfate is activated by a combination of temperature increase, UV-light or transition metals, such as Fe(II) and Fe(III):EDDS (Reactions 13–14 and Figs. 6 and 7). Once activated, it generates the strongly oxidizing sulfate radicals ($SO_4^{\bullet-}$), following the reactions below (Reactions 1–12): [Sánchez-Polo et al., 2013]

$$S_2O_8^{2-} + h\vartheta \rightarrow 2SO_4^{2-} \quad (1)$$

$$SO_4^{\bullet-} + RH_2 \rightarrow SO_4^{2-} + H^+ + RH^{\bullet} \quad (2)$$

$$RH^{\bullet} + S_2O_8^{2-} \rightarrow R + SO_4^{2-} + H^+ + SO_4^{\bullet-} \quad (3)$$

$$SO_4^{\bullet-} + RH \rightarrow R^{\bullet} + SO_4^{2-} + H^+ \quad (4)$$

$$2R^{\bullet} \rightarrow RR\ (dimer) \quad (5)$$

$$SO_4^{\bullet-} + H_2O \rightarrow HSO_4^- + O \quad (6)$$

$$HSO_4^- \rightarrow H^+ + SO_4^{2-} \quad (7)$$

$$^{\bullet}OH + S_2O_8^{2-} \rightarrow HSO_4^- + SO_4^{\bullet-} + \frac{1}{2}O_2 \quad (8)$$

$$SO_4^{\bullet-} + {}^{\bullet}OH \rightarrow HSO_4^- + \frac{1}{2}O_2 \quad (9)$$

$$^{\bullet}O_2H \rightarrow H_2O_2 \quad (10)$$

$$^{\bullet}OH + H_2O_2 \rightarrow H_2O + {}^{\bullet}O_2H \quad (11)$$

$$S_2O_8^{2-} + H_2O_2 \rightarrow 2H^+ + 2SO_4^{2-} + O_2 \quad (12)$$

$$Fe(III) : EDDS + h\vartheta \rightarrow Fe^{2+} + EDDS_{ox} \quad (13)$$

$$Fe^{2+} + S_2O_8^{2-} \rightarrow SO_4^{\bullet-} + SO_4^{2-} + Fe^{3+} \quad (14)$$

These radicals can react with MCs due to their high redox potential, which is similar to $^{\bullet}OH$, but they preferentially work by electron transfer. This preference provides a synergistic effect for MC elimination, while reinforcing the Fenton process by lowering the water pH with sulfuric acid generated by Reaction 12. [Wu et al., 2015; Lian et al., 2017] Therefore, it would be a good alternative to classic photo-Fenton at pH 3, as reaction rates would be higher due to the presence of both hydroxyl and sulfate radicals. However, results of persulfate as an oxidizing agent at pH 3 did not clearly improve the MC degradation rate

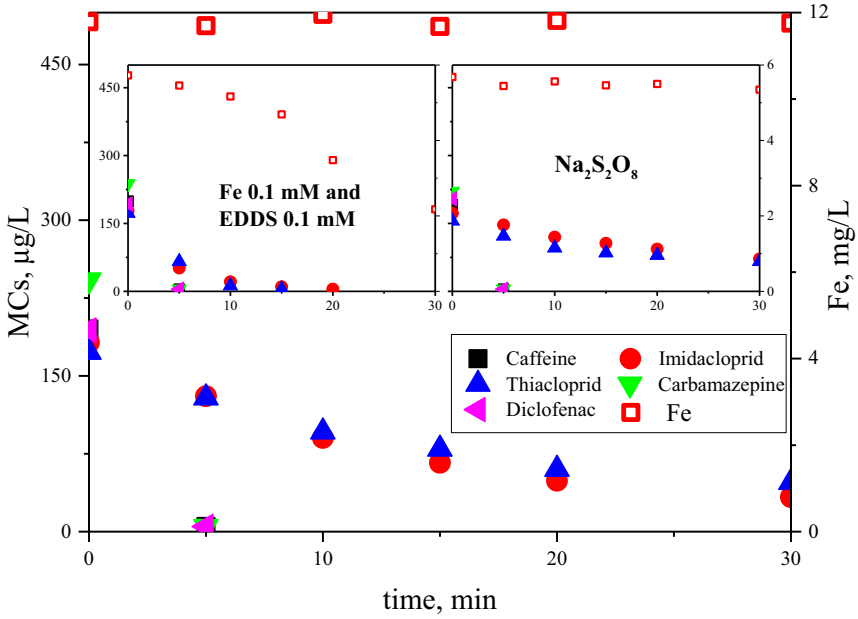

Fig. 7. MC concentrations and dissolved iron evolution in C1 during solar photo-Fenton at natural pH (Fe 0.20 mM, EDDS 0.20 mM and 1.50 mM H_2O_2). The insets show the results with Fe 0.1 mM and EDDS 0.10 mM and the same ratio with persulfate (1.50 mM) as the oxidizing agent.

(Fig. 6). *CAF, CAR and DIC elimination* to LOQ (5 μg/L) was attained *in less than 5 min.* First order kinetic constant were in general lower than classic photo-Fenton at pH 3: 0.753 min^{-1}, 0.021 min^{-1}, 0.028 min^{-1}, 0.774 min^{-1}, 0.706 min^{-1} for CAF, IMI, THI, CAR and DIC, respectively. *Consumption of persulfate was 10% of the starting amount. Only* 90% of IMI and THI was eliminated after 30 min of treatment, and although these elimination rates are similar to those with H_2O_2, IMI was more persistent with persulfate as the oxidizing agent.

3.2.4. Effect of operating parameters on solar photo-Fenton tertiary treatment at natural pH

The effect of operating parameters such as Fe(III):EDDS concentration (0.20 mM iron or half EDDS, 0.10 mM) and persulfate as the oxidizing agent instead of H_2O_2 was also evaluated in solar photo-Fenton treatment of C1 at natural pH.

When the concentration of iron was doubled (0.20 mM, Fe:EDDS [1:1]), as seen in Fig. 7 and compared to 0.10 mM of iron (Fig. 5, Fe:EDDS [1:2]), *CAF, CAR and DIC reached* LOQ (5 μg/L) *in less than 5* min. Elimination of 80% IMI and 70% THI was also attained after 30 min. First order kinetic constant were 0.732 min^{-1}, 0.061 min^{-1}, 0.048 min^{-1}, 0.776 min^{-1}, 0.732 min^{-1} for CAF, IMI, THI, CAR and DIC, respectively. Furthermore, no iron precipitation was detected and H_2O_2 *consumption* was 1.35 mM after 30 min. The higher concentration of iron resulted in a negative effect on elimination of IMI and THI at natural pH. It may be concluded that increasing the iron concentration to 0.20 mM increased the total concentration of generated $^{\bullet}OH$. The $^{\bullet}OH$ surplus could then recombine to H_2O_2 (Reaction 10–11), which at natural pH, promoted the formation of H_2O and O_2. Potential competition of EDDS with the MCs for the oxidant, also increasing the dissolved organic carbon, seems to be unlikely, as no iron precipitation was observed, showing that the Fe(III):EDDS complex was stable during the experiment.

As seen in the inset in Fig. 7, with only half of the EDDS concentration (0.10 mM), *CAF, CAR and DIC were* eliminated to LOQ (5 μg/L) *in less than 5 min.* Elimination of over 90% of the sum of MCs was achieved after 15 min and H_2O_2 *consumption was* 0.70 mM, ending at 1.00 mM after 30 min. First order kinetic constant were 0.737 min^{-1}, 0.189 min^{-1}, 0.241 min^{-1}, 0.772 min^{-1}, 0.731 min^{-1} for CAF, IMI, THI, CAR and DIC, respectively. Compared to the basic experimental parameters (Fe 0.10 mM, EDDS 0.20 mM and 1.50 mM H_2O_2) shown in Fig. 5, the elimination rates were slightly better, however, this time with lower H_2O_2 consumption. In this case iron precipitation was observed earlier starting after 10 min, with a total loss of 0.02 mM at 15 min and 0.07 mM at 30 min. The loss of iron is well justified, as at the lower concentrations of EDDS, Fe(III) is complexed for shorter times. Thus, the lower EDDS concentration had a positive effect (lower dissolved organic carbon, and therefore less competition with MCs for the oxidants) on MC elimination at natural pH.

Finally, by applying persulfate as the oxidizing agent at natural pH (inset, Fig. 7), *CAF, CAR and DIC* to LOQ (5.0 μg/L) were eliminated in less than 5 min. The maximum elimination of 60% of the recalcitrant IMI and THI was attained after 30 min. Elimination rates were similar to the curve of the basic experimental parameters using H_2O_2 at neutral pH as observed in Fig. 5. IMI persistence was similar, although to a lesser extent, to results at pH 3 with persulfate as the oxidizing agent compared to H_2O_2 at natural pH. First order kinetic constant were 0.729 min^{-1}, 0.031 min^{-1}, 0.033 min^{-1}, 0.758 min^{-1}, 0.742 min^{-1} for CAF, IMI, THI, CAR and DIC, respectively. Total persulfate consumption was 0.85 mM, which is significantly higher than in the experiment performed at pH 3, but no substantial improvement in MC degradation was observed compared to H_2O_2 at neutral pH.

The reduction of toxicity of MCs present in water and effluents by solar photo-Fenton has been widely studied in many recent studies, as for example [Miralles-Cuevas et al., 2017; Hong et al., 2020; Gonçalves et al., 2020; Michael et al., 2019], including application of a selected battery of bioassays in vivo (algal growth inhibition test) and in vitro, endocrine disruptors tests (androgenic/glucocorticoid activity and estrogenicity) and cytotoxicity tests [Rivas Ibáñez et al., 2017]. The overall conclusion was that MCs removal is in concordance with the toxicity reduction shown by many bioanalytical tools. Therefore, in our research we did not delve into this study as there is abundant information regarding the evolution of toxicity during photo-Fenton solar treatment.

4. Conclusions

The first increase in salinity and system pressure had a negligible influence on the order of permeability and NF membrane selectivity when natural water was employed as the matrix. Nevertheless, the key factor in such systems for preconcentration before a tertiary treatment is the concentration factor (CF) required, which strongly depends on water matrix salinity and capacity operating pressure.

The higher MC degradation rates in C1 with Fe(III):EDDS at natural pH than at pH 3 could not be justified by a lack of oxidizing radicals caused by low iron concentration, but rather due to the high concentration of sulfate in C1 which scavenged hydroxyl and other radicals.

When persulfate was used instead of hydrogen peroxide, the mediating radicals for oxidation of the MCs, $^{\bullet}OH$ and $SO_4^{\bullet-}$, had different elimination efficiencies. Whereas persulfate was inefficient for the selected MCs, overproduction of radicals lowered the elimination efficiency, perhaps by inducing scavenging and the formation of other (less active) radical species (e.g., chloride radicals) and recombination.

Solar photo-Fenton was demonstrated to be able to degrade, not only MCs present in the concentrate stream of a NF system, but also rapidly eliminate any residual MCs that could be present in the permeate streams after long NF operation. Fe(III):EDDS at circumneutral pH applied to salinized natural water was able to remove MCs from NF streams as quickly as classical photo-Fenton at acid pH, or even faster. This effect reinforces the proposal for using Fe(III):EDDS at natural pH for treating NF concentrates and also for polishing NF permeates when NF membranes are operated under extreme conditions, leaving MCs in the permeate due to increasing salinity in UWWTP effluents.

CRediT authorship contribution statement

Dennis Deemter: Investigation, Writing - original draft. **Isabel Oller:** Conceptualization, Formal analysis, Methodology, Validation, Writing - review & editing, Supervision, Funding acquisition, Project administration. **Ana M. Amat:** Conceptualization, Formal analysis, Methodology, Validation, Supervision, Writing - review & editing, Supervision, Funding acquisition, Project administration. **Sixto Malato:** Writing - review & editing.

Declaration of competing interest

The authors declare that they have no known competing financial interests or personal relationships that could have appeared to influence the work reported in this paper.

Acknowledgements

This paper is part of a project that received funding from the European Union's Horizon 2020 Research and Innovation Programme under Marie Skłodowska-Curie Grant Agreement No 765860. Dennis Deemter would like to thank the staff at the Plataforma Solar de Almería. The authors wish to thank the Spanish Ministry of Science, Innovation and Universities (MCIU), AEI and FEDER for funding under the CalypSol Project (Reference: RTI2018-097997-B-C32 and RTI2018-097997-B-C31).

Appendix A. Supplementary data

Supplementary data to this article can be found online at https://doi.org/10.1016/j.scitotenv.2020.143593.

References

Abdel-Fatah, M.A., 2018. Nanofiltration systems and applications in wastewater treatment: review article. Ain Shams Eng J 9 (4), 3077–3092. https://doi.org/10.1016/j.asej.2018.08.001.

Ahile, U.J., Wuana, R.A., Itodo, A.U., Sha'Ato, R., Dantas, R.F., 2020. A review on the use of chelating agents as an alternative to promote photo-Fenton at neutral pH: current trends, knowledge gap and future studies. Sci. Total Environ. 710, 134872. https://doi.org/10.1016/j.scitotenv.2019.134872.

Bi, F., Zhao, H., Zhou, Z., Zhang, L., Chen, H., Gao, C., 2016. Optimal design of nanofiltration system for surface water treatment. Chin. J. Chem. Eng. 24 (12), 1674–1679. https://doi.org/10.1016/j.cjche.2016.05.012.

Brandt, A., Gorenflo, A., Siede, R., Meixner, M., Büchler, R., 2016. The neonicotinoids thiacloprid, imidacloprid, and clothianidin affect the immunocompetence of honey bees (Apis mellifera L.). J. Insect Physiol. 86, 40–47. https://doi.org/10.1016/j.jinsphys.2016.01.001.

Capocelli, M., Prisciandaro, M., Piemonte, V., Barba, D., 2019. A technical-economical approach to promote the water treatment & reuse processes. J. Clean. Prod. 207, 85–96. https://doi.org/10.1016/J.JCLEPRO.2018.09.135.

Clarizia, L., Russo, D., Di Somma, I., Marotta, R., Andreozzi, R., 2017. Homogeneous photo-Fenton processes at near neutral pH: a review. Appl. Catal. B Environ. 209, 3581. https://doi.org/10.1016/j.apcatb.2017.03.011.

Costa, E.P., Roccamante, M., Amorim, C.C., Oller, I., Sánchez Pérez, J.A., Malato, S., 2020. New trend on open solar photoreactors to treat micropollutants by photo-Fenton at circumneutral pH: increasing optical pathway. Chem. Eng. J. 385, 123982. https://doi.org/10.1016/j.cej.2019.123982.

De Laat, J., Truong Le, G., Legube, B., 2004. A comparative study of the effects of chloride, sulfate and nitrate ions on the rates of decomposition of H2O2 and organic compounds by Fe(II)/H2O2 and Fe(III)/H2O 2. Chemosphere 55 (5), 715–723. https://doi.org/10.1016/j.chemosphere. 2003.11.021.

Dong, W., Sun, S.P., Yang, X., et al., 2019. Enhanced emerging pharmaceuticals removal in wastewater after biotreatment by a low-pressure UVA/FeIII-EDDS/H2O2 process under neutral pH conditions. Chem. Eng. J. 366, 539–549. https://doi.org/10.1016/j.cej.2019.02.109.

Eggen, R.I.L., Hollender, J., Joss, A., Schärer, M., Stamm, C., 2014. Reducing the discharge of micropollutants in the aquatic environment: the benefits of upgrading wastewater treatment plants. Environ. Sci. Technol. 48, 7683–7689. https://doi.org/10.1021/es500907n.

Gallego-Schmid, A., Tarpani, R.R.Z., Miralles-Cuevas, S., Cabrera-Reina, A., Malato, S., Azapagic, A., 2019. Environmental assessment of solar photo-Fenton processes in combination with nanofiltration for the removal of micro-contaminants from real wastewaters. Sci. Total Environ. 650, 2210–2220. https://doi.org/10.1016/J.SCITOTENV.2018.09.361.

Gonçalves, B.R., Guimarães, R.O., Batista, L.L., Ueira-Vieira, C., Starling, M.C.V.M., Trovó, A.G., 2020. Reducing toxicity and antimicrobial activity of a pesticide mixture via photo-Fenton in different aqueous matrices using iron complexes. Sci. Total Environ. 740, 140152. https://doi.org/10.1016/j.scitotenv.2020.140152.

Hong, M., Wang, Y., Lu, G., 2020. UV-Fenton degradation of diclofenac, sulpiride, sulfamethoxazole and sulfisomidine: degradation mechanisms, transformation products, toxicity evolution and effect of real water matrix. Chemosphere 258, 127351. https://doi.org/10.1016/j.chemosphere.2020.127351.

Ike, I.A., Linden, K.G., Orbell, J.D., Duke, M., 2018. Critical review of the science and sustainability of persulphate advanced oxidation processes. Chem. Eng. J. 338, 651–669. https://doi.org/10.1016/j.cej.2018.01.034.

Jaber, S., Leremboure, M., Thery, V., Delort, A.M., Mailhot, G., 2020. Mechanism of photochemical degradation of Fe(III)-EDDS complex. J. Photochem. Photobio. A: Chem. https://doi.org/10.1016/j.jphotochem.2020.112646.

Janssens, R., Cristovao, M.B., Bronze, M.R., Crespo, J.G., Pereira, V.J., Luis, P., 2019. Coupling of nanofiltration and UV, UV/TiO2 and UV/H2O2 processes for the removal of anticancer drugs from real secondary wastewater effluent. J Environ Chem Eng 7 (5), 103351. https://doi.org/10.1016/J.JECE.2019.103351.

Kanakaraju, D., Glass, B.D., Oelgemöller, M., 2018. Advanced oxidation process-mediated removal of pharmaceuticals from water: a review. J. Environ. Manag. 219, 189–207. https://doi.org/10.1016/j.jenvman.2018.04.103.

Kessler, S.C., Tiedeken, E.J., Simcock, K.L., 2015. Bees prefer foods containing neonicotinoid pesticides. Nature 521 (7550), 74–76. https://doi.org/10.1038/nature14414.

Kim, S., Chu, K.H., Al-Hamadani, Y.A.J., Park, C.M., Jang, M., Kim, D.-H., Yu, M., Heo, J., Yoon, Y., 2018. Removal of contaminants of emerging concern by membranes in water and wastewater: a review. Chem. Eng. J. 335, 896–914. https://doi.org/10.1016/j.cej.2017.11.044.

Klamerth, N., Malato, S., Maldonado, M.I., Agüera, A., Fernández-Alba, A.R., 2010. Application of photo-Fenton as a tertiary treatment of emerging contaminants in municipal wastewater. Environ. Sci. Technol. 44, 1792–1798. https://doi.org/10.1016/j.watres.2012.11.008.

Lado Ribeiro, A.R., Moreira, N.F.F., Li Puma, G., Silva, A.M.T., 2019. Impact of water matrix on the removal of micropollutants by advanced oxidation technologies. Chem. Eng. J. 363, 155–173. https://doi.org/10.1016/j.cej.2019.01.080.

Li, K., Wang, J., Liu, J., Wei, Y., Chen, M., 2016. Advanced treatment of municipal wastewater by nanofiltration: operational optimization and membrane fouling analysis. J. Environ. Sci. 43, 106–117. https://doi.org/10.1016/j.jes.2015.09.007.

Lian, L., Yao, B., Hou, S., Fang, J., Yan, S., Song, W., 2017. Kinetic study of hydroxyl and sulfate radical-mediated oxidation of pharmaceuticals in wastewater effluents. Environ. Sci. Technol. 51 (5), 2954–2962. https://doi.org/10.1021/acs.est.6b05536.

Liang, C., Huang, C.F., Mohanty, N., Kurakalva, R.M., 2008. A rapid spectrophotometric determination of persulfate anion in ISCO. Chemosphere 73 (9), 1540–1543. https://doi.org/10.1016/j.chemosphere.2008.08.043.

McGinnis, M., Sun, C., Dudley, S., Gan, J., 2019. Effect of low-dose, repeated exposure of contaminants of emerging concern on plant development and hormone homeostasis. Environ. Pollut. 252, 706–714. https://doi.org/10.1016/J.ENVPOL.2019.05.159.

Mendret, J., Azais, A., Favier, T., Brosillon, S., 2019. Urban wastewater reuse using a coupling between nanofiltration and ozonation: techno-economic assessment. Chem. Eng. Res. Des. 145, 19–28. https://doi.org/10.1016/J.CHERD.2019.02.034.

Meschke, K., Hansen, N., Hofmann, R., Haseneder, R., Repke, J.-U., 2020. Influence of process parameters on separation performance of strategic elements by polymeric nanofiltration membranes. Sep. Purif. Technol. 235, 116186. https://doi.org/10.1016/J.SEPPUR.2019.116186.

Michael, S.G., Michael-Kordatou, I., Beretsou, V.G., Jäger, T., Michael, C., Schwartz, T., Fatta-Kassinos, D., 2019. Solar photo-Fenton oxidation followed by adsorption on activated carbon for the minimisation of antibiotic resistance determinants and toxicity present in urban wastewater. Appl. Catal. B Environ. 244, 871–880. https://doi.org/10.1016/j.apcatb.2018.12.030.

Miklos, D.B., Remy, C., Jekel, M., Linden, K.J., Drewes, J.E., Hübner, U., 2018. Evaluation of advanced oxidation processes for water and wastewater treatment – a critical review. Water Res. 139, 118–131. https://doi.org/10.1016/j.watres.2018.03.042.

Miralles-Cuevas, S., Arqués, A., Maldonado, M.I., Sánchez-Pérez, J.A., Malato Rodríguez, S., 2013. Combined nanofiltration and photo-Fenton treatment of water containing micropollutants. Chem. Eng. J. https://doi.org/10.1016/j.cej.2012.09.068.

Miralles-Cuevas, S., Oller, I., Pérez, J.A.S., Malato, S., 2014. Application of solar photo-Fenton at circumneutral pH to nanofiltration concentrates for removal of pharmaceuticals in MWTP effluents. Environ. Sci. Pollut. Res. https://doi.org/10.1007/s11356-014-2871-2.

Miralles-Cuevas, S., Oller, I., Agüera, A., Sánchez Pérez, J.A., Malato, S., 2017. Strategies for reducing cost by using solar photo-Fenton treatment combined with nanofiltration to remove microcontaminants in real municipal effluents: toxicity and economic assessment. Chem. Eng. J. 318, 161–170.

Patel, M., Kumar, R., Kishor, K., Mlsna, T., Pittman, C.U., Mohan, D., 2019. Pharmaceuticals of emerging concern in aquatic systems: chemistry, occurrence, effects, and removal methods. Chem. Rev. 119, 3510–3673. https://doi.org/10.1021/acs.chemrev.8b00299.

Petrović, M., Gonzalez, S., Barceló, D., 2003. Analysis and removal of emerging contaminants in wastewater and drinking water. TrAC Trends Anal. Chem. 22 (10), 685–696. https://doi.org/10.1016/S0165-9936(03)01105-1.

Pico, Y., Belenguer, V., Corcellas, C., 2019. Contaminants of emerging concern in freshwater fish from four Spanish Rivers. Sci. Total Environ. 659, 1186–1198. https://doi.org/10.1016/J.SCITOTENV.2018.12.366.

Rasheed, T., Bilal, M., Nabeel, F., Adeel, M., Iqbal, H.M.N., 2019. Environmentally-related contaminants of high concern: potential sources and analytical modalities for detection, quantification, and treatment. Environ. Int. 122, 52–66. https://doi.org/10.1016/J.ENVINT.2018.11.038.

Ricart, S., Rico, A.M., 2019. Assessing technical and social driving factors of water reuse in agriculture: a review on risks, regulation and the yuck factor. Agric. Water Manag. 217, 426–439. https://doi.org/10.1016/J.AGWAT.2019.03.017.

Rivas Ibáñez, G., Bittner, M., Toušová, Z., Campos-Mañas, M.C., Agüera, A., Casas López, J.L., Sánchez Pérez, J.A., Hilscherová, K., 2017. Does micropollutant removal by solar photo-Fenton reduce ecotoxicity in municipal wastewater? A comprehensive study at pilot scale open reactors: municipal wastewater toxicity removal by solar photo-Fenton at neutral pH. J. Chem. Technol. Biotechnol. 92, 2114–2122. https://doi.org/10.1002/jctb.5212.

Rizzo, L., Malato, S., Antakyali, D., et al., 2019. Consolidated vs new advanced treatment methods for the removal of contaminants of emerging concern from urban wastewater. Sci. Total Environ. 655, 986–1008. https://doi.org/10.1016/J.SCITOTENV.2018.11.265.

Sánchez-Polo, M., Abdel daiem, M.M., Ocampo-Pérez, R., Rivera-Utrilla, J., Mota, A.J., 2013. Comparative study of the photodegradation of bisphenol A by HO, SO4- and CO3-/HCO3 radicals in aqueous phase. Sci. Total Environ. 463-464, 423–431. https://doi.org/10.1016/j.scitotenv.2013.06.012.

Shi, X., Tal, G., Hankins, N.P., Gitis, V., 2014. Fouling and cleaning of ultrafiltration membranes: a review. J Water Process Eng. https://doi.org/10.1016/j.jwpe.2014.04.003.

Silva, P., Livingston, A.G., 2006. Effect of solute concentration and mass transfer limitations on transport in organic solvent nanofiltration — partially rejected solute. Membrane Science 280, 889–898. https://doi.org/10.1016/j.memsci.2006.03.008.

Song, Y., Qin, W., Li, T., Hu, Q., Gao, C., 2018. The role of nanofiltration membrane surface charge on the scale-prone ions concentration polarization for low or medium saline water softening. Desalination 432, 81–88. https://doi.org/10.1016/j.desal.2018.01.013.

Soriano-Molina, P., García Sánchez, J.L., Alfano, O.M., Conte, L.O., Malato, S., Sánchez Pérez, J.A., 2018. Mechanistic modeling of solar photo-Fenton process with Fe3+-EDDS at neutral pH. Appl. Catal. B Environ. 233, 234–242. https://doi.org/10.1016/j.apcatb.2018.04.005.

Soriano-Molina, P., Plaza-Bolaños, P., Lorenzo, A., Agüera, A., García Sánchez, J.L., Malato, S., Sánchez Pérez, J.A., 2019. Assessment of solar raceway pond reactors for removal of contaminants of emerging concern by photo-Fenton at circumneutral pH from very different municipal wastewater effluents. Chem. Eng. J. 366, 141–149. https://doi.org/10.1016/j.cej.2019.02.074.

Tandy, S., Ammann, A., Schulin, R., Nowack, B., 2006. Biodegradation and speciation of residual SS-ethylenediaminedisuccinic acid (EDDS) in soil solution left after soil washing. Environ. Pollut. 142 (2), 191–199. https://doi.org/10.1016/j.envpol.2005.10.013.

UN DESA, 2019. World Population Prospects 2019.

Voigt, I., Richter, H., Stahn, M., et al., 2019. Scale-up of ceramic nanofiltration membranes to meet large scale applications. Sep. Purif. Technol. 215, 329–334. https://doi.org/10.1016/J.SEPPUR.2019.01.023.

Wang, J., Wang, S., 2018b. Activation of persulfate (PS) and peroxymonosulfate (PMS) and application for the degradation of emerging contaminants. Chem. Eng. J. 334, 1502–1517. https://doi.org/10.1016/j.cej.2017.11.059.
Wang, S., Wang, J., 2018a. Trimethoprim degradation by Fenton and Fe(II)-activated persulfate processes. Chemosphere 191, 97–105. https://doi.org/10.1016/j.chemosphere.2017.10.040.
Wang, X., Dong, W., Brigante, M., Mailhot, G., 2019. Hydroxyl and sulfate radicals activated by Fe(III)-EDDS/UV: comparison of their degradation efficiencies and influence of critical parameters. Appl. Catal. B Environ. 245, 271–278. https://doi.org/10.1016/j.apcatb.2018.12.052.
Wu, Y., Bianco, A., Brigante, M., et al., 2015. Sulfate radical photogeneration using Fe-EDDS: influence of critical parameters and naturally occurring scavengers. Environ. Sci. Technol. 49 (24), 14343–14349. https://doi.org/10.1021/acs.est.5b03316.
Zapata, A., Oller, I., Bizani, E., Sánchez-Pérez, J.A., Maldonado, M.I., Malato, S., 2009. Evaluation of operational parameters involved in solar photo-Fenton degradation of a commercial pesticide mixture. Catal. Today 144, 94–99. https://doi.org/10.1016/j.cattod.2008.12.030.
Zhang, M., Guan, K., Ji, Y., Liu, G., Jin, W., Xu, N., 2019. Controllable ion transport by surface-charged graphene oxide membrane. Nat. Commun. 10, 1253. https://doi.org/10.1038/s41467-019-09286-8.
Zhang, Y., Zhou, M., 2019. A critical review of the application of chelating agents to enable Fenton and Fenton-like reactions at high pH values. J. Hazard. Mater. 362, 436–450. https://doi.org/10.1016/j.jhazmat.
Zhang, Y., Wang, L., Sun, W., Hu, Y., Tang, H., 2020. Membrane technologies for Li+/Mg2+ separation from salt-lake brines and seawater: a comprehensive review. J. Ind. Eng. Chem. 81, 7–23. https://doi.org/10.1016/j.jiec.2019.09.002018.09.035.